frontiers | Frontiers in Physics

ORIGINAL RESEARCH
published: 13 May 2022
doi: 10.3389/fphy.2022.877577

Ion Microbeam Studies of Charge Transport in Semiconductor Radiation Detectors With Three-Dimensional Structures: An Example of LGAD

Milko Jakšić[1], Andreo Crnjac[1], Gregor Kramberger[2], Miloš Manojlović[3], Gordana Laštovička-Medin[3] and Mauricio Rodriguez Ramos[1]*

[1]*Ruđer Bošković Institute, Division of Experimental Physics, Zagreb, Croatia,* [2]*Jožef Stefan Institute, Ljubljana, Slovenia,* [3]*Faculty of Natural Sciences and Mathematics, University of Montenegro, Podgorica, Montenegro*

The development of semiconductor detectors with an increased tolerance to high radiation levels often results in devices that deviate significantly from those of the classical design with planar electrodes. Decreasing the charge drift distance and/or introducing localised charge multiplication volumes are two detector development strategies that are often used in an attempt to increase the device radiation hardness. However, such approaches result in a more complex three-dimensional distribution of electrodes and sensitive detector volumes, which presents a challenge for the microscopic characterisation of charge transport properties. IBIC (ion beam-induced charge) is one of the available microscopic characterisation techniques that utilises focused, MeV energy range ions to probe charge transport. Here we used IBIC to probe different detector depths by varying the ion energy and/or angle of incidence and to probe certain detector regions by ions of the same range but with different stopping powers. These investigations are particularly important for studying low gain avalanche diode (LGAD) detectors, where measured interpad distances change with proton energy and where an increased carrier density results in changes in the charge multiplication, which are studied in this work.

Keywords: ion microprobe, IBIC, charge collection efficiency, semiconductor detectors, LGAD, gain suppression

OPEN ACCESS

Edited by:
Gabriele Giacomini, Brookhaven National Laboratory (DOE), United States

Reviewed by:
Francesco Moscatelli, National Research Council (CNR), Italy
Ian Harding, Brookhaven National Laboratory (DOE), United States

****Correspondence:***
Milko Jakšić
jaksic@irb.hr

Specialty section:
This article was submitted to Radiation Detectors and Imaging, a section of the journal Frontiers in Physics

Received: *16 February 2022*
Accepted: *20 April 2022*
Published: *13 May 2022*

Citation:
Jakšić M, Crnjac A, Kramberger G, Manojlović M, Laštovička-Medin G and Ramos MR (2022) Ion Microbeam Studies of Charge Transport in Semiconductor Radiation Detectors With Three-Dimensional Structures: An Example of LGAD. Front. Phys. 10:877577. doi: 10.3389/fphy.2022.877577

INTRODUCTION

The increased demand for position-sensitive radiation sensing with enhanced radiation hardness and very good time resolution has paved the way for new solutions and new technologies of semiconductor detector manufacturing, often resulting in a complex 3D (three dimensional) structure of the final device [1, 2]. Good examples of such detectors are monolithic silicon pixel detectors [3, 4], multipixel silicon LGAD detectors [5–8], detectors with 3D electrodes (silicon and diamond) [9, 10], etc. Studying the charge transport in such structures is most frequently accomplished today by different variations of the TCT (transient current technique) technique, which uses laser light to create charge carriers in certain detector regions, generally through the small openings in electrodes that enable passage of light [11, 12]. Other techniques are based on the induction of charge carriers from different radiation sources, such as electrons from accelerators, radioactive sources (e.g., betas from Sr90) or electron microscopy (SEM-EBIC) [13], focused X-rays from tube or synchrotron light, and finally a variety of heavier charge particles from radioisotope sources (e.g., alphas from Am241) or accelerators (IBIC) [14–17].

However, to probe the charge transport in all three dimensions, only edge TCT and two-photon absorption TCT can offer some possibilities, with limitations concerning the non-transparency of contacts and limits in terms of spatial resolution. The use of an ion microbeam however, offers clear advantages in that respect, as ions are transmitted through contacts and could have a micrometre spatial resolution in all dimensions. This is a great advantage to fully characterise the formation of a signal when charge carriers are created at different coordinates of the detector. Therefore, in this work we focus on exploring the capabilities of using MeV energy ions and the ion beam induced charge (IBIC) technique in an attempt to extract information about charge transport at the microscopic scale and in all three dimensions. This approach is based on the possibility of an ion microprobe focusing system that provides an (x,y) coordinate for each penetrating ion with micrometre ionisation precision. Furthermore, using the capability of the accelerator facility to provide different ions and different ion energies, IBIC probing of the third coordinate, i.e., the depth (z), could also be performed. It is important to note here that the energy loss for ions of few MeV energy increases by decreasing ion energy and therefore the majority of charge carriers from ionisation are generated in the detector at the end of the ion range (Bragg peak). We have therefore explored different approaches of IBIC characterisation by changing the analysis depth of the same ion type having different energies and ranges and/or by changing the specific energy loss (ionisation density) at particular detector depths by using different ion species and their respective energies. To demonstrate these capabilities, we selected several prototypes of LGAD detectors for further studies.

MATERIALS AND METHODS

LGAD Detectors

The LGAD range of silicon sensors, originally developed at CNM (Centro Nacional de Microelectrónica) [7], features an internal gain layer that amplifies rather small signals produced by the minimum ionising particles (MIP). Contrary to an APD (Avalanche Photo Diode), which has higher signal amplification and is primarily developed for detection of visible light photons, the signal gain in LGAD does not need to be high, since the primary application is for the detection of MIPs. Under these conditions, only electrons contribute to amplification due to the much higher impact ionisation coefficients than holes. Additionally, since LGAD is relatively thin (tens of micrometres), the short drift times of charge carriers enable excellent timing properties. Timing resolution as low as tens of picoseconds is particularly important for applications in experiments at high luminosity colliders.

For this investigation, the integration of LGAD into a segmented multipixel array is of additional interest, since it also enables positional (x,y) sensitivity. In the current stage of development, the typical separation of the pixel pads for the standard LGAD, is between 30 and 100 μm. This is rather large and therefore, pixel sizes have to be of the mm^2 area to maintain sufficiently high fill factors of multipixel arrays and also to accommodate the complex electronics needed for precise timing measurements. The typical thickness of the sensitive LGAD volume is most often around 50 μm, which is a good compromise between good timing capabilities and large enough primary ionization. As seen in the sketch presented in **Figure 1A**, a high electric field is formed in a multiplication layer at a junction of a highly doped n++ area and highly doped gain p + -layer. The distance between the neighbouring gain p + -layers is defined as the nominal interpad distance. To reduce the electric field at the lateral edges of this multiplication layer, a junction termination edge (JTE) is also implanted. The gap between pixels is covered by the silicon oxide layer but also contains a p-stop region that isolates the neighbouring electrodes. It is obvious that the structure of this region will have a significant influence on the effective interpad distance; therefore, it would be beneficial if the variation in the inefficient area could be measured as a function of depth as well. It has to be noted however, that there are other segmentation strategies that can be applied to decrease the interpad distance, one being the most promising is the Trench-Isolated—TI-LGAD [18]. More details about the different aspects of the LGAD structure, characteristics, radiation hardness and application areas can be found in the literature [5].

Three specific previously non-irradiated samples were investigated by IBIC in this work. All were produced by Hamamatsu (HPK) with an equally thick 50 μm sensitive depth. Sample A is 2x2 pixel structure HPK W28 2x2 IP5-SE3, sample B is the same as A but single pad, sample C is 2x2 pixel structure HPK W36 2x2 IP7-SE3. Differences between the two multipad samples are the nominal interpad distance (W28–70 μm; W36–90 μm) and the depletion voltage of the gain layer (W28—54.5 V, W36—51 V). From the IV curve presented also in **Figure 1B**, one can see that the two critical voltages when depletion of the gain layer (V_{GL}) and depletion of the full detector (V_{FD}) are achieved are in the region between 50 and 60 V. This information is important for studies related to the behaviour of the LGAD detector gain as a function of the bias voltage.

IBIC Depth Profiling

IBIC is an established ion microprobe technique that has been used for measuring the charge transport properties in semiconductor radiation detectors and other electronic devices for more than 3 decades [14–17]. It is based on the injection of charge pairs by ionisation produced along the trajectories of single ions of the MeV energy range. The ion beam is focused on micrometre spot sizes in a microprobe system by a multiplet of quadrupole magnets (doublets, triplets, and quadruplets). For the purpose of IBIC, which is one of several other single ion microprobe techniques [19] ion currents have to be reduced to values below 1 fA by reduction of object and collimator slit openings. Focused ions are raster scanned over the test structure using a magnetic or electrostatic scanner that controls the ion positioning over the areas in sizes between the micrometre and millimetre range. The scan size is calibrated for each ion and its respective energy using the metal mesh of known pitch size, which is placed in front of

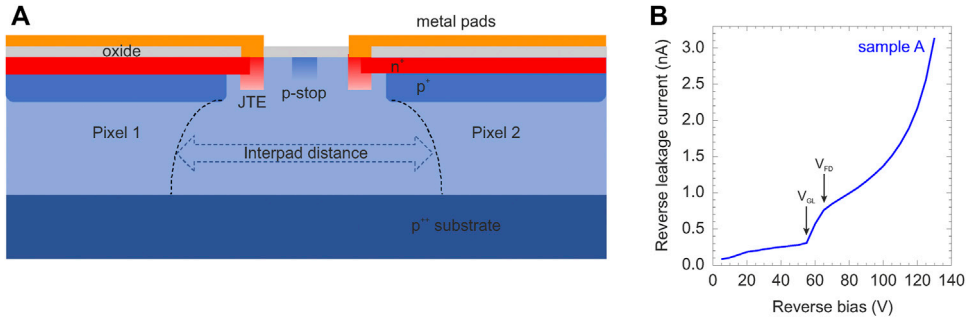

FIGURE 1 | (A) Sketch of the LGAD detector with indicated edge of pixels. **(B)** I/V curve for sample A with V_{GL} and V_{FD} positions.

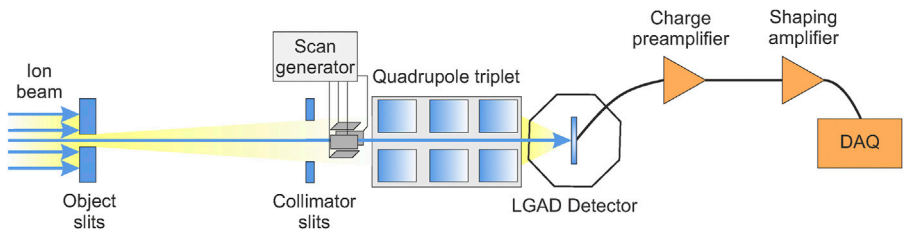

FIGURE 2 | Schematic presentation of the ion microprobe focussing and scanning system with IBIC pulse processing electronic chain. Charge sensitive preamplifier used was Ortec 142A, while the amplifier was Ortec 570. Data acquisition was based on Canberra ADC 8701 and in house made SPECTOR software.

the silicon surface barrier detector used otherwise for the performance of STIM imaging [20, 21].

An important part of the IBIC system is pulse processing electronics, since the current pulse induced at the electrodes of the test structure by a single ion must be amplified (typically by a charge-sensitive preamplifier), recorded and correlated with the position of an ion impact. To calibrate the charge collection efficiency (CCE) of the detector structure being tested, and consequently its gain (for LGAD), the same electronic chain used for IBIC is used with the Canberra PIPS (passivated implanted planar silicon) detector of 300 μm thickness. This detector, used otherwise for STIM experiments, was exposed directly to the ion beam, assuming its 100% CCE. A schematic presentation of the ion microprobe system and the IBIC experimental setup is shown in **Figure 2**.

Since the calibrated scanning system provides the (x,y) coordinates for each recorded event, enabling 2D IBIC imaging, the additional possibility of the setup to select different ions and their respective energies could be used to probe the charge transport at a different range of test structures depths (z coordinate). In the case of the RBI microprobe, a large range of detector depths could be studied; for silicon material and protons, this range spans from only 1 micrometre (120 keV) up to 500 micrometres (8 MeV), which can be provided by one of the two available tandem accelerators.

Another important characteristic of the ion microprobe system is its capability to significantly increase the microbeam current by several orders of magnitude to values that induce radiation damage in the test structure. Under such circumstances, one type of ion could be used both as a damaging beam and as a beam for probing the charge collection properties [22].

Unfortunately, despite the great potential to probe drastically different ranges of detector structures, changing the ion type and/or its energy and the performance of IBIC at each of these ion/energy combinations will also require refocusing. This is generally a time-consuming process that is rarely used in practice. We have therefore explored different strategies that would enable faster changes in the ion energies and thus a simpler performance of the IBIC "depth profiling".

The simplest approach of IBIC probing different depths of detector structures is by using different ions of the same magnetic rigidity. In such cases, once focused, the microprobe system does not require further refocusing [23, 24] for the second ion of the same rigidity. For the RBI facility, which has two tandem accelerators (1.0 and 6.0 MV), available sputtering negative ion sources could easily provide different ion beams of the same rigidity. For switching the system between the two types of ions, only the terminal voltage adjustment would be needed, which is done in a matter of minutes. We are therefore showing here a simple solution by using two ion types, namely, H^- and Li^-, which were produced in a sputtering ion source from a LiH target and injected into the accelerator system. The combination of the same rigidity ions we used here were: 1.41 MeV energy protons, having 27.5 μm range in silicon, and 1.81 MeV energy lithium ($^7Li^{3+}$) ions, having 4.32 μm range in silicon. As an example, we show on **Figure 3**, IBIC scans for these two ions in the LGAD interpad area of sample A. In all cases 128 × 128 pixels were used for imaging, however the absolute size of the scan area was changed and is

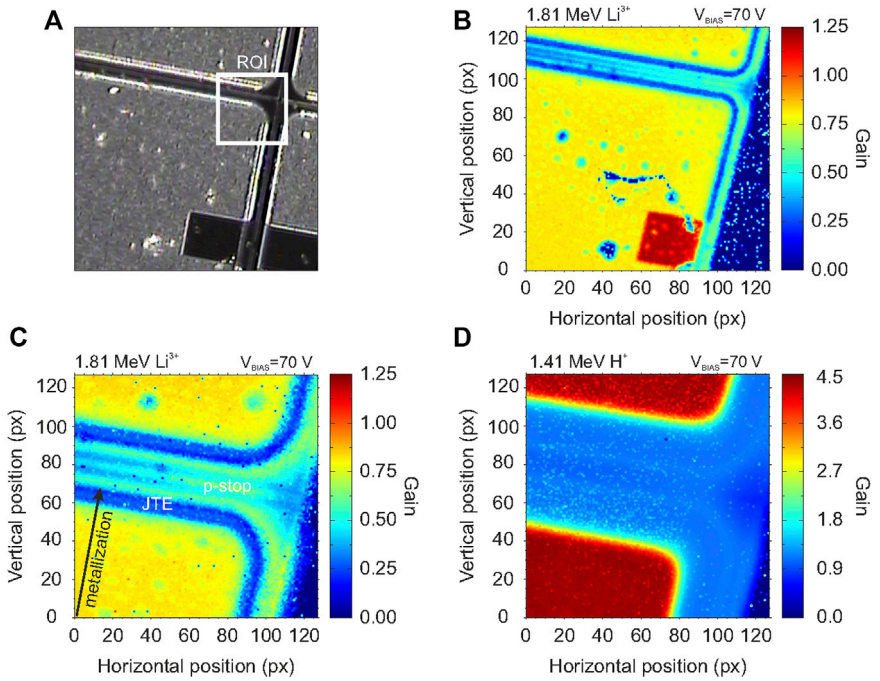

FIGURE 3 | (A) Optical image of the intergap region of sample A with opening in metallization for laser light tests (at bottom right); **(B)** 1.81 MeV ^{7}Li ion IBIC image of 570 × 570 μm^2 scan area; **(C)** 1.81 MeV ^{7}Li ion IBIC image of 190 × 190 μm^2 scan area, arrow is indicating extension of the metallization contact for the lower pad; **(D)** 1.41 MeV proton beam IBIC of the same area as in **(C)**. Small patches of low efficiency visible at **(B,C)** are due to the dust particles at detector surface.

indicated by the scale bar. As shown in figure, significant changes in the observed structure could be observed by two ions of very different ranges. For the short-range Li ion, the IBIC image reveals the surface structures of the interpad region (metallisation, JTE, p-stop gain). The ion range is however too small to produce any gain in signal. For the long-range protons, only two regions (gain and no-gain regions at the interpad) in the detector depth could be seen, indicating clearly the edge defined by the electric field lines that lead charge carriers towards the charge multiplication regions.

Unfortunately, flexibility in selecting the appropriate ion range for an IBIC measurement with the above approach is rather limited and is applicable only for certain combinations of ions. Furthermore, frequent changes in ion species also require changes in ion source operating conditions, which is again not practical or fast. Therefore, in this work we used two other approaches based on the application of only one ion type and on subsequent changes in its energy.

To avoid the need for refocusing, we first tested the performance of IBIC without the use of focusing quadrupoles and thus using a collimated beam only. In the case of the RBI microprobe system, collimation is performed by a pair of slits (object and collimator) separated by 6 m and with openings for both slits set to approximately 10 micrometres. These openings generally give beam currents in the fA range, which is suitable for IBIC, while the existing microprobe beam scanning system can be used as well. Changes in the ion energy are performed by recalculation of all ion-optical components (deflectors, quadrupoles, analyser magnets), which can be done within a 10-min time. However, this approach is only used when a low microbeam spatial resolution (≅10 μm) is sufficient, e.g., when the gain-to-voltage dependence for one particular LGAD pixel and for each ion penetration depth is being studied.

In most of the other cases, when a high spatial resolution of the microbeam has to be maintained for all the ion energies, quadrupole system refocusing is needed. Refocusing is performed manually in most microprobe systems by observing the beam shape on the scintillation screen while changing the quadrupole currents. Consequently, during this process the IBIC

TABLE 1 | List of the experimental conditions used in 5 experimental sessions of IBIC measurements performed on 3 different LGAD samples explained in text.

Ion	Energy (MeV)	Sample	Angle of Incidence	Range in Si (μm)	Bragg Peak Mode (μm)
H	1.41	A	0	27.8	-
Li	1.81	A	0	4.32	-
H	1.80	A	0	40	-
H	1.41	A	0	28	-
H	0.9	A	0	14	-
H	0.56	A	0	7	-
C	18	B	0	17.7	-
C	11.52	B	0	11	-
C	14	C	0	14	10.2
He	3	C	0	12.5	10.2
H	0.75	C	0	11	10.2
H	1.41	A	0	29	27.8
H	1.80	A	45	32	27.8

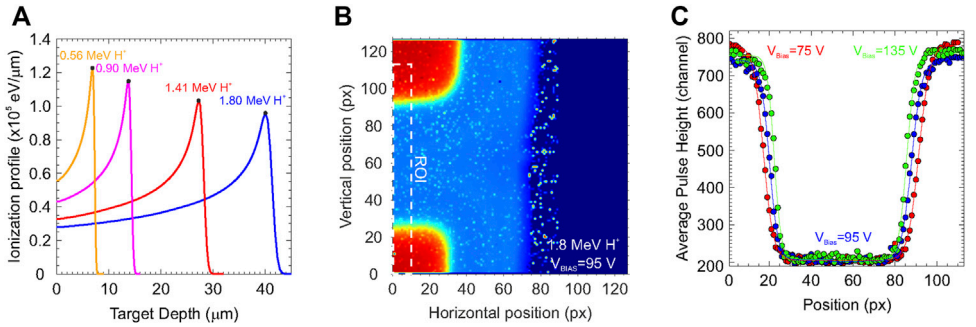

FIGURE 4 | (A) Ionization profiles for 4 proton energies used to measure the interpad gap distance. **(B)** IBIC areal scan (175 × 175 μm^2) for sample A obtained by 1.8 MeV protons and 95 V bias. **(C)** CCE profiles for 1.8 MeV protons between the two active pixels fitted by an error function for 3 different biases.

sample must be moved. To avoid manual focusing at each of the ion energies, we tested an alternative approach based on the calibration of quadrupole magnetic fields measured by a Gauss meter. In this approach, after initial demagnetisation of the quadrupoles, the beam has been focused manually only at the lowest beam energy. For each of the subsequent ion beam energies, magnetic fields were recalculated, quadrupole currents were changed, and measurements were performed for each of the energies. To minimise possible focus degradation in these subsequent field adjustments, a low demagnification, long working distance, quadrupole doublet microprobe setup was used. Under these circumstances, small imperfections in beam focus adjustments are less important since the low divergence setup of the object and collimator apertures was used (<100 μsr). In most of the energies adjusted in this way, beam resolution could be maintained around the 1 micrometre figure. In **Table 1** we summarise all ions and respective energies used in the presented studies, along with their corresponding ranges in silicon.

RESULTS AND DISCUSSION

From the previously shown IBIC images obtained with two different ion energies (**Figure 3**), it is obvious that the complex 3D structure of the LGAD detector can be revealed with a series of areal (x,y) scans performed by subsequent changes in the ion energies providing a depth (z) sensitivity analysis. It is also expected that the use of different ions that create significantly different densities of charge carriers along their trajectory could influence the gain of the LGAD detector pixel. Several combinations of ion energies, ion species and the geometry of IBIC experiments have been performed (**Table 1**) and are explained in detail in the following sections, together with discussions of results that correspond to certain characteristics of LGAD detectors.

Changes in the Ion Energy

Interpad Distance

One of the most important characteristics of any radiation detector is certainly the one that defines its absolute detection efficiency, which in most cases is related to the sensitive detector volume. In the case of multipixel LGAD detectors, this information is difficult to obtain, since the edges of pixels change with depth due to the curvatures in the electric field lines, along which charge carriers drift towards the gain layer (see **Figure 1**). Since LGAD detectors are primarily used for the detection of minimum ionising particles (MIPs), which only create sufficiently high (and fast) signals when primarily generated electrons arrive into the gain region, the effective pixel size is determined entirely by the amplification volume, while the signals from the interpad region are too small to contribute to the detector efficiency.

To explore how this interpad distance changes with depth, a series of IBIC measurements using different proton energies and a normal incidence were performed. The ion energy loss (ionisation profiles) as a function of depth is presented in **Figure 4A** for all ion (proton) energies used. It is important to note here that in LGAD, the main contribution to the gain signal comes from electrons through the process of impact ionisation. Since holes do not contribute to the signal by the impact ionisation process, the ionisation curves have to be observed in a different manner. First, electrons formed before the gain layer (up to approximately 5 μm from the surface) do not contribute to the signal amplification at all. This is also visible in the IBIC images shown in **Figure 3** performed by Li ions that stopped completely in the first 4 microns with no gain being observed. Second, for the rest of the LGAD depth, and following the Shockley–Ramo theorem, it is evident that the highest contribution to the current signal will come from the ionisation events that took place at the deepest detector parts. Under such conditions, the ionisation profile for electrons is more dominated by the Bragg peak; therefore, one can claim, at least for the purpose of calculating the interpad distance, that events that contribute to the gain are, on average, coming from the depths of the Bragg peak position.

For each of the energies (exp. 1 of **Table 1**), scans between two pads of the approximately 200 × 200 μm area were performed, recording the data for each of the operating voltages between 50 and 150 V. To maintain equal operating conditions in these two neighbouring pixels, both were connected to a single pulse processing electronic chain based on the charge sensitive

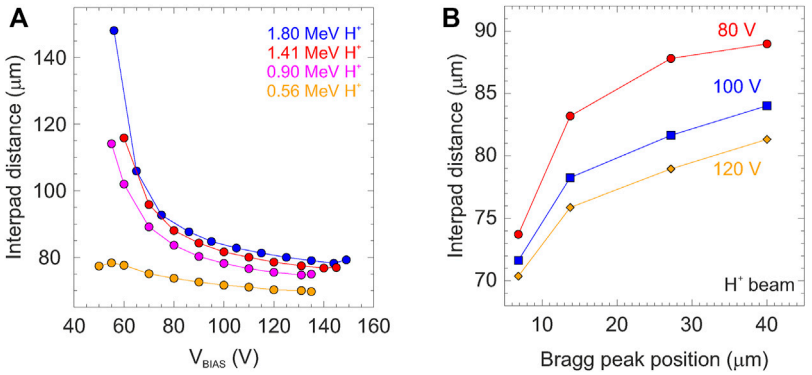

FIGURE 5 | (A) Interpad distance measurements results for sample A, shown as a function of proton energy used. **(B)** Interpad distance measured for 3 bias voltages shown as a function of probing depth represented by a median of the ionization profile Bragg peak.

preamplifier Ortec 142A. An example of the experimental CCE profiles between the two adjacent pixels is shown in **Figure 4B** for several bias voltages, together with fits using the error function. Statistical error of these fits, that are used to obtain the final interpad distance value, is in all cases smaller than 0.5 μm.

The resulting interpad distances obtained for all 4 proton energies, measured as a function of the bias, are shown in **Figure 5A**. This distance is strongly dependent on the bias voltage, with the smallest values being those for the highest voltages. Additionally, the smallest range protons (0.56 MeV), with a Bragg peak maximum position at only 6.5 μm, which is just after the end of the gain p + -layer, give the smallest measured distances. These experimental values are grouped at approximately 70 μm for the highest bias voltages, which is also the nominal interpad distance for this particular sample. In **Figure 5B**, we also show measured values of the effective distance (measured by 4 proton energies) in relation to the position of the Bragg peak maximum for each of the proton energies. For the deepest penetrating protons (1.8 MeV), the interpad distance for the maximum bias is approximately 80 μm. This dependence is in qualitative agreement with modelled electric fields for such devices [25], showing that the IBIC technique can be easily adopted for the precise determination of intragap distances at different LGAD depths.

Gain Suppression

It is known that LGAD detectors respond in different ways to radiation of different specific energy losses, with lower gains being observed for the detection of highly ionising particles. This phenomenon is known as the gain suppression effect. Until now, the mechanisms of gain suppression were investigated in different ways, for example, by comparing the response between the minimum ionising particles (MIP) and laser light (TCT), whose intensity can be changed to simulate particles with a higher specific energy loss [26, 27]. Additionally, the same effect has been investigated with alpha particles from radioisotope sources. In this work, we used data obtained during the above explained investigation of the interpad gap distance, since the observed gain-to-voltage dependence as a function of the proton penetration range exhibits features that can only be explained by the gain suppression mechanism.

To fully understand the origin of gain suppression, it is important to note that the primary charge carriers from ionisation induced by a single proton arrive at the very small volume of the gain layer where multiplication by impact ionisation occurs. High charge densities induce a local reduction of the electric field (electric field screening), resulting in a reduced gain of the LGAD detector. In quantity, the gain measured for highly ionising particles, such as protons, is much smaller than the gain for the minimum ionising particles (MIPs). As shown in **Figure 6A**, the gain for protons is of the order of 3-4, while MIPs for the same detector will induce a gain on the order of 20. However, in the same figure it can be seen that unlike MIPs, for which gain increases monotonically with voltage up to the breakdown voltage V_{BD}, the highest gain for protons is actually observed for low voltages around the V_{FD}. This "peak" is less pronounced for shorter penetration protons and is qualitatively similar for carbon ions, as shown in **Figure 6B**.

The fact that the highest gain is observed at low voltages can be explained as follows. At voltages around the V_{FD} value, the electric field in the drift region is still quite low, and therefore the charge carriers drift slowly towards the gain layer. Under such circumstances, diffusion of the charge carriers (electrons) becomes important, since the volume of the charge cloud arriving at the gain layer is much larger than in cases with higher bias voltages. Therefore, the charge density in the gain layer is smaller, the electric field screening effect decreases, and eventually the gain is higher. Since the time needed for charge carriers to arrive at the gain layer is larger at low voltages for deeper penetrating ions, this 'peak' in the gain-to-voltage dependence is more pronounced compared to measurement with lower energy ions.

To confirm this hypothesis, charge carrier trajectories in the drift region of LGAD were simulated for two different bias voltages and 1.81 MeV protons. The results of the simulation obtained by the open source KDETsim code [28] are presented in **Figure 7**. The simulation clearly shows that the diffusion of charge carriers during their passage

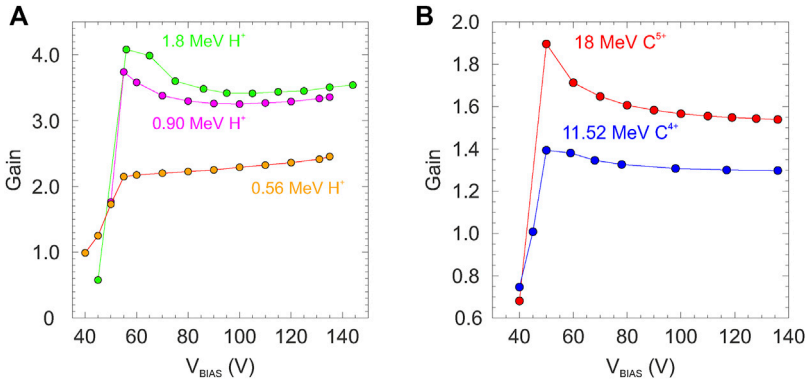

FIGURE 6 | (A) Gain to voltage dependences obtained by three different proton energies on sample A. **(B)** Gain for two different carbon ion energies on sample B.

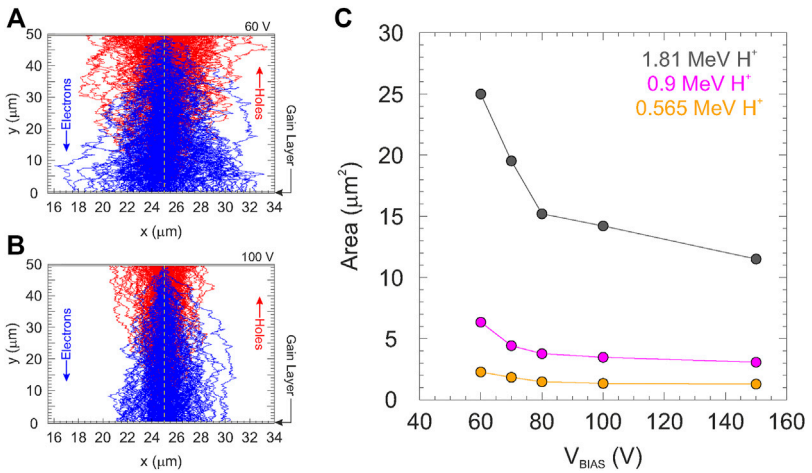

FIGURE 7 | Simulations of charge carrier trajectories in silicon exposed to protons of 1.8 MeV energy, for two different biases, 60 V **(A)** and 100 V **(B)**. Simulations are used to calculate FWHM of charge cloud spread at x = 0 and subsequently the areal spread of charge cloud in gain layer. At right **(C)**, dependence of areal spread on bias voltage for three proton energies is given.

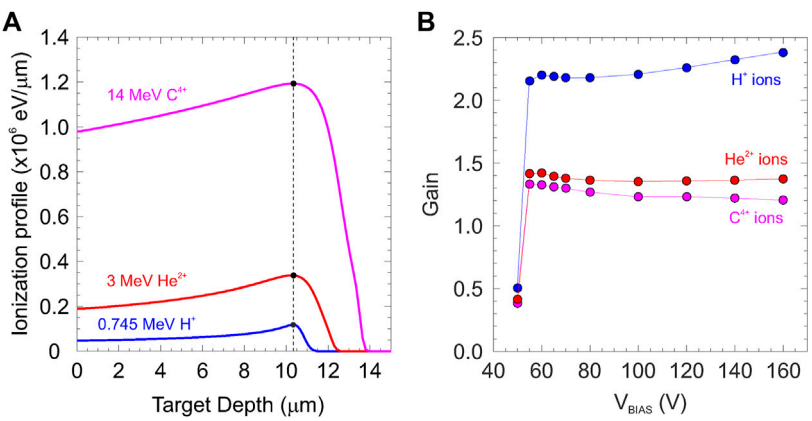

FIGURE 8 | (A) Ionization profiles for three ions (H, He and C) having maximum of ionization at the same depth in silicon. **(B)** Gain in LGAD sample C, shown as a function of bias voltage for these ions.

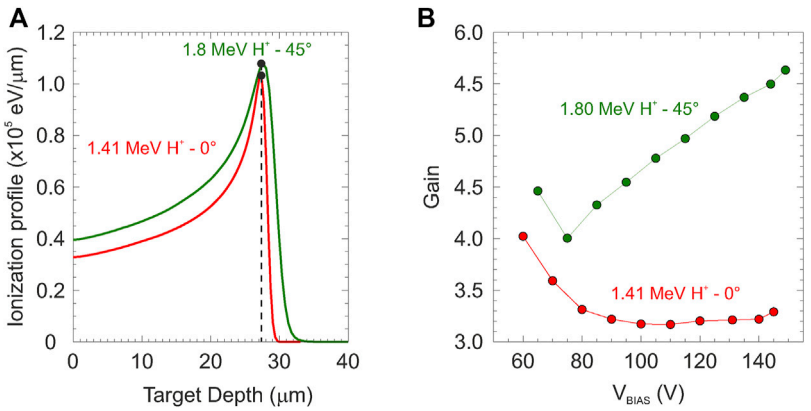

FIGURE 9 | (A) Ionization profiles for normal incidence of 1.41 MeV protons and for 1.8 MeV protons with 45^0 incidence angle. **(B)** Dependence of gain on bias voltage for sample A.

towards the gain layer is significant for low electric fields in the drift region of LGAD. By increasing the voltage, the charge carriers drift faster, and the spatial density of charge carriers increases, resulting in a higher electric field screening effect. For smaller penetration ranges, the diffusion contribution will be less pronounced since the drift time of charge carriers is shorter. Therefore, the gain "peak", which is visible for deep penetration ions, is less pronounced for the low-range ions.

Changes in the Ion Type

The effect of electric field screening and subsequent gain suppression in LGAD can also be studied by exposing the detector to different ion species as they produce different ionisation densities along their trajectory in the detector. The three ions selected for this experiment were 0.75 MeV protons, 3 MeV He ions and 14 MeV C ions, which have similar ranges but significantly different energy loss values. The energies of ions have been selected to have the maximum energy loss curve placed at the same depth of approximately 10 micrometres, as seen in **Figure 8A**. This adjustment was important to simplify the interpretation of the results, since all three ions will induce qualitatively similar depth distributions for the charge carriers (electrons). Therefore, the travel path and velocity of created carriers that will be moving towards the high electric field region will be the same. However, since the amount of charge carriers created along the ion track will be significantly different when comparing these three ions, the charge density arriving at the gain layer will be different, and will subsequently affect the final gain in a different way.

The results of these three measurements are shown in **Figure 8B**, and as expected, the lowest gain in the LGAD test sample was observed for the highest ionisation particles, namely, the 14 MeV C ions. These data can be easily used to model the electric field screening, since in the first approximation, the only difference between the three cases is the number of charge pairs initially created.

Changes in the Angle of Incidence

The ability to change the angle under which an ion microbeam penetrates into the detector has often been used when determining the thicknesses of inactive detector surface layers, such as metallisation, SiO2 protection, and Si dead layers [29–31]. By appropriate selection of the ion energy and angle of incidence, inactive layer thicknesses could be easily measured. This type of experiment has already been performed in the case of LGAD to measure, among others, the thickness of the surface metallisation as well as the thickness of the active layer of detector [32].

In the case of this study, however, we have used IBIC measurements under different angles to further investigate the gain suppression mechanism. Two different ion incidence angles have been proposed to confirm the earlier assumption that widening the charge cloud entering the gain layer (due to diffusion of the charge carriers) reduces the electric field screening. We therefore selected a proton beam that enters either vertically (along the z-axis) towards the detector surface or under an angle of 45 degrees. However, as we have already shown that ions of different ranges in LGAD respond in a different way, we adjusted the energy of inclined ion incidence in a way to have the same range as ions with normal incidence. This has been achieved for 1.41 MeV protons (normal incidence) and 1.8 MeV protons (45° incidence angle), as shown in **Figure 9A**. The ionisation depth profile (along the z-axis) is of a similar shape between these two modes. However, for the 45° angle, the (x,y) projection of the charge cloud arriving at the gain layer will be spread in one dimension (x) to more than 25 micrometres, and therefore, its density and subsequently the electric field screening will be much smaller.

As expected, a comparison of the results obtained by these two IBIC probing angles, shown in **Figure 9B**, reveals a large difference. The gain-to-voltage dependence for inclined angle probing by protons is now more similar to the behaviour that is obtained by minimum ionising particles with a characteristic increase in the gain by the voltage. This clearly shows that a reduction in the density of the charge cloud will minimise the electric field screening and reduce the gain suppression.

Nevertheless, at the lowest bias value measured, just above the V_{FD} value, the increase in efficiency for 45° angle of incidence is also noticed, as is the case for the normal incidence. Thus, the final shape of the gain-to-voltage dependence for inclined angle IBIC probing is a superposition of the characteristic shape obtained for MIPs (at high voltages) and the strongly screened shape obtained for normal incidence of protons (at lower voltages). A further simulation of the charge carrier dynamics when different proton incidence angles are used could provide a reliable data source for quantitative modelling of the gain suppression mechanism.

CONCLUSION

The main aim of the presented work was to investigate different approaches to perform an IBIC experiment that provides insight into the physics of detectors whose response is changing in all 3 dimensions and on the microscopic scale. The LGAD range of detectors was shown to be a good test case, as its response changes across the surface (xy) due to the discrete dimension of pixel pads and interpad gaps, while its response along the depth (z) changes due to the gain layer positioned just beneath the detector surface where charge multiplication occurs.

The performance of IBIC probing at different ion energies was used to measure the depth profile of the interpad gap between the adjacent gain layer implants. It changes with the ion range and is, as expected, the highest for the deepest penetration ion, while for the shallow probing ions, the gap reaches its nominal value. The performance of this approach to study the dependence of the interpad distance on other parameters, such as the temperature and radiation damage [33], could be easily applied in a routine characterisation of LGAD detector samples. In addition, the use of short-range heavier ions also showed excellent possibilities for identifying the distribution and thicknesses of inefficient surface layers in LGAD detectors.

Probing different depths also revealed the effect of electric field screening, namely, the existence of maximum gain at low bias voltages (just above the V_{FD}) and for deep penetrating ions, in which cases the gain is anomalously higher when compared to the high bias values. We have explained this behaviour *via* diffusion of charge carriers (electrons) that travel towards the gain layer, subsequent enlargement of the charge cloud, a decrease in the electric field screening and finally an increased gain for these conditions. Simulations of charge carrier trajectories confirmed this hypothesis.

The performance of IBIC probing using different ions and therefore different ionisation depth profiles was used to confirm the effects of electric field screening. We used three different ions (H, He and C) with qualitatively similar ionisation profiles. As expected, the C ions showed almost complete suppression of the gain due to the large ionisation density produced along the ion track. Much smaller gain suppression was measured for inclined IBIC probing *via* protons. Only under these circumstances did the LGAD test samples show the characteristic shape of the gain-to-voltage dependence, which increased constantly with voltage.

Despite the fact that ion microbeams have only been occasionally used for the characterisation of complex detector prototypes, the presented series of investigations showed that IBIC capabilities could offer a good alternative to laser beam-based techniques, which will have certain limitations in the characterisation of charge transport in detectors with underlying 3D structures. Apart from the LGAD detector characterised in this work, this has already been proven through IBIC analyses of other detectors, including 3D diamond detectors [34, 35]. In this work, we also proposed how possible problems in the time-consuming refocusing of different ion beams can be avoided, which will enable a more efficient IBIC characterisation of complex detector structures.

Finally, it must be added that ion microprobe systems could also be used, apart from IBIC probing, to induce radiation damage (e.g., by MeV protons traversing the detector thickness completely) in specific detector parts or to induce single event effects (SEEs) by heavy ions in neighbouring redout electronics. Beyond the scope of this work is also the possibility of a microprobe system to inject fast ions in certain detector zones and records current transients, namely, the time resolved IBIC (TRIBIC), which could also offer certain advantages over the conventional laser TCT.

DATA AVAILABILITY STATEMENT

The raw data supporting the conclusions of this article will be made available by the authors, without undue reservation.

AUTHOR CONTRIBUTIONS

MJ, GL-M, and GK contributed to conception of the LGAD study; MJ, AC, and MR contributed to the design and planning of the IBIC experiments; AC, MR, GL-M, and MM conducted ion microprobe measurements; AC, MR, and MM performed data analysis; AC, GK, and MM performed charge transport modelling; MR prepared the figures; all authors discussed the experimental results; and MJ wrote the first draft of the manuscript. All authors contributed to manuscript revision and read and approved the submitted version.

FUNDING

This project received funding from the European Union's Horizon 2020 Research and Innovation programme under grant agreement No 101004761. MJ, AC, and MR acknowledge financial support from the European Regional Development Fund for the 'Center of Excellence for Advanced Materials and Sensing Devices' (Grant No. KK.01.1.1.01.0001) and for the the Competitiveness and Cohesion Operational Programme (Grant No. KK.01.1.1.06). GL-M and MJ wish to acknowledge support provided by the IAEA within the framework of Coordinated Research Projects G42008 and F11020. Part of the research has been funded through the Slovenian Research Agency project J1-1699.

REFERENCES

1. Karmakar A, Wang J, Prinzie J, De Smedt V, Leroux P. A Review of Semiconductor Based Ionising Radiation Sensors Used in Harsh Radiation Environments and Their Applications. *Radiation* (2021) 1:194–217. doi:10.3390/radiation1030018
2. Seidel S. Silicon Strip and Pixel Detectors for Particle Physics Experiments. *Phys Rep* (2019) 828:1–34. doi:10.1016/j.physrep.2019.09.003
3. Snoeys W. Monolithic Pixel Detectors for High Energy Physics. *Nucl Instrum Methods Phys Res Sect A Accel Spectrom Detect Assoc Equip* (2013) 731:125–30. doi:10.1016/j.nima.2013.05.073
4. Deveaux M. Progress on the Radiation Tolerance of CMOS Monolithic Active Pixel Sensors. *J. Inst.* (2019) 14:R11001. doi:10.1088/1748-0221/14/11/R11001
5. Giacomini G. Fabrication of Silicon Sensors Based on Low-Gain Avalanche Diodes. *Front. Phys.* (2021) 9:618621. doi:10.3389/fphy.2021.618621
6. Cartiglia N, Arcidiacono R, Borghi G, Boscardin M, Costa M, Galloway Z, et al. LGAD Designs for Future Particle Trackers. *Nucl Instrum Methods Phys Res Sect A Accel Spectrom Detect Assoc Equip* (2020) 979:164383. doi:10.1016/j.nima.2020.164383
7. Pellegrini G, Fernández-Martínez P, Baselga M, Fleta C, Flores D, Greco V, et al. Technology Developments and First Measurements of Low Gain Avalanche Detectors (LGAD) for High Energy Physics Applications. *Nucl Instrum Methods Phys Res Sect A Accel Spectrom Detect Assoc Equip* (2014) 765:12–6. doi:10.1016/j.nima.2014.06.008
8. Currás E. Low Gain Avalanche Detectors for 4-dimensional Tracking Applications in Severe Radiation Environments. *JPS Conf. Proc.* (2021) 34: 010015. doi:10.7566/JPSCP.34.010015
9. Lange J, Giannini G, Grinstein S, Manna M, Pellegrini G, Quirion D, et al. Radiation Hardness of Small-Pitch 3D Pixel Sensors up to a Fluence of 3×1016 Neq/cm2. *J. Inst.* (2018) 13:P09009. doi:10.1088/1748-0221/13/09/P09009
10. Anderlini L, Bellini M, Bizzeti A, Cardini A, Ciaranfi R, Corsi C, et al. Fabrication and Characterisation of 3D Diamond Pixel Detectors with Timing Capabilities. *Front. Phys.* (2020) 8:474. doi:10.3389/fphy.2020.589844
11. Kramberger G, Cindro V, Mandic I, Mikuz M, Milovanovic M, Zavrtanik M, et al. Investigation of Irradiated Silicon Detectors by Edge-TCT. *IEEE Trans. Nucl. Sci.* (2010) 57:2294–302. doi:10.1109/TNS.2010.2051957
12. Wiehe M, Garcia MF, Moll M, Montero R, Palomo FR, Vila I, et al. Development of a Tabletop Setup for the Transient Current Technique Using Two-Photon Absorption in Silicon Particle Detectors. *IEEE Trans. Nucl. Sci.* (2021) 68:220–8. doi:10.1109/TNS.2020.3044489
13. Leamy HJ. Charge Collection Scanning Electron Microscopy. *J Appl Phys* (1982) 53:R51–R80. doi:10.1063/1.331667
14. Angell D, Marsh BB, Cue N, Miao JW. Charge Collection Ion Microscopy: Imaging of Defects in Semiconductors with a Positive Ion Microbeam. *Nucl Instrum Methods Phys Res Sect B Beam Interact Mater Atoms* (1989) 44:172–8. doi:10.1016/0168-583X(89)90424-2
15. Breese MBH, Vittone E, Vizkelethy G, Sellin PJ. A Review of Ion Beam Induced Charge Microscopy. *Nucl Instrum Methods Phys Res Sect B Beam Interact Mater Atoms* (2007) 264:345–60. doi:10.1016/j.nimb.2007.09.031
16. Vittone E. Semiconductor Characterization by Scanning Ion Beam Induced Charge (IBIC) Microscopy. *ISRN Mater Sci* (2013) 2013:1–17. Hindawi. doi:10.1155/2013/637608
17. Manfredotti C, Fizzotti F, Vittone E, Boero M, Polesello P, Galassini S, et al. IBIC Investigations on CVD Diamond. *Nucl Instrum Methods Phys Res Sect B Beam Interact Mater Atoms* (1995) 100:133–40. doi:10.1016/0168-583X(95)00268-5
18. Paternoster G, Borghi G, Arcidiacono R, Boscardin M, Cartiglia N, Centis Vignali M, et al. Novel Strategies for Fine-Segmented Low Gain Avalanche Diodes. *Nucl Instrum Methods Phys Res Sect A Accel Spectrom Detect Assoc Equip* (2021) 987:164840. doi:10.1016/j.nima.2020.164840
19. Jeynes C, Webb RP, Lohstroh A. Ion Beam Analysis: A Century of Exploiting the Electronic and Nuclear Structure of the Atom for Materials Characterisation. *Rev. Accl. Sci. Tech.* (2011) 04:41–82. doi:10.1142/S1793626811000483
20. Breese MBH, Landsberg JP, King PJC, Grime GW, Watt F. Applications of Scanning Transmission Ion Microscopy. *Nucl Instrum Methods Phys Res Sect B Beam Interact Mater Atoms* (1992) 64:505–11. doi:10.1016/0168-583X(92)95524-U
21. Aguer P, Alves LC, Barberet P, Gontier E, Incerti S, Michelet-Habchi C, et al. Skin Morphology and Layer Identification Using Different STIM Geometries. *Nucl Instrum Methods Phys Res Sect B Beam Interact Mater Atoms* (2005) 231: 292–9. doi:10.1016/j.nimb.2005.01.073
22. Grilj V, Skukan N, Jakšić M, Pomorski M, Kada W, Kamiya T, et al. The Evaluation of Radiation Damage Parameter for CVD Diamond. *Nucl Instrum Methods Phys Res Sect B Beam Interact Mater Atoms* (2016) 372:161–4. doi:10.1016/j.nimb.2015.12.046
23. Jakšić M, Fazinić S, Tadić T, Bogovac B, Bogdanović I, Pastuović Ž. IBIC Study of Charge Collection Properties in Si(Li) Detectors. *Nucl. Instr. Meth.* (1998) B136-138:1327–32. doi:10.1016/s0168-583x(97)00848-3
24. Jakšić M, Pastuović Ž, Tadić T. New Developments in IBIC for the Study of Charge Transport Properties of Radiation Detector Materials. *Nucl. Instr. Meth.* (1999) 158:458–63. doi:10.1016/s0168-583x(99)00321-3
25. Mandurrino M, Arcidiacono R, Boscardin M, Cartiglia N, Dalla Betta G-F, Ferrero M, et al. Analysis and Numerical Design of Resistive AC-Coupled Silicon Detectors (RSD) for 4D Particle Tracking. *Nucl Instrum Methods Phys Res Sect A Accel Spectrom Detect Assoc Equip* (2020) 959:163479. doi:10.1016/j.nima.2020.163479
26. Curras E, Fernandez M, Moll M. *Gain Suppression Mechanism Observed in Low Gain Avalanche Detectors*. Nucl Instr Meth(2022) A1031:166530. doi:10.1016/j.nima.2020.163479
27. McKeon JB, Chindalore G, Hareland SA, Shih W-K, Wang C, Tasch AF, et al. Experimental Determination of Electron and Hole Mobilities in MOS Accumulation Layers. *IEEE Electron Device Lett.* (1997) 18(5):200–2. doi:10.1109/55.568762
28. Kramberger G, Cindro V, Mikuž M. Signals in non-irradiated and irradiated single-sided silicon detectors, *Nucl. Instr. and Meth.* (2001) 550–557. Available at: www.kdetsim.org. doi:10.1016/S0168-9002(00)00776-2
29. Yang C, Jamieson DN, Hearne SM, Pakes CI, Rout B, Gauja E, et al. Ion-beam-induced-charge Characterisation of Particle Detectors. *Nucl Instrum Methods Phys Res Sect B Beam Interact Mater Atoms* (2002) 190:212–6. doi:10.1016/S0168-583X(02)00456-1
30. Giudice AL, Garino Y, Manfredotti C, Rigato V, Vittone E. Angle Resolved IBIC Analysis of 4H-SiC Schottky Diodes. *Nucl Instrum Methods Phys Res Sect B Beam Interact Mater Atoms* (2006) 249:213–6. doi:10.1016/j.nimb.2006.03.168
31. Pezzarossa M, Cepparrone E, Cosic D, Jakšić M, Provatas G, Vićentijević M, et al. Polychromatic Angle Resolved IBIC Analysis of Silicon Power Diodes. *Nucl Instrum Methods Phys Res Sect B Beam Interact Mater Atoms* (2021) 488: 50–63. doi:10.1016/j.nimb.2020.12.006
32. Jiménez-Ramos MC, García López J, García Osuna A, Vila I, Currás E, Jaramillo R, et al. Study of Ionization Charge Density-Induced Gain Suppression in LGADs. *Sensors* (2022) 22:1080. doi:10.3390/s22031080
33. Bharthuar S, Ott J, Helariutta K, Litichevskyi V, Brücken E, Gädda A, et al. Study of Interpad-Gap of HPK 3.1 Production LGADs with Transient Current Technique. *Nucl Instrum Methods Phys Res Sect A Accel Spectrom Detect Assoc Equip* (2020) 979:164494. doi:10.1016/j.nima.2020.164494
34. Forcolin GT, Grilj V, Hamilton B, Li L, McGowan M, Murphy SA, et al. Study of a 3D Diamond Detector with Photon and Proton Micro-beams. *Diam Relat Mater* (2016) 65:75–82. doi:10.1016/j.diamond.2016.02.005
35. Girolami M, Conte G, Trucchi DM, Bellucci A, Oliva P, Kononenko T, et al. Investigation with β-particles and Protons of Buried Graphite Pillars in Single-Crystal CVD Diamond. *Diam Relat Mater* (2018) 84:1–10. doi:10.1016/j.diamond.2018.02.014

Conflict of Interest: The authors declare that the research was conducted in the absence of any commercial or financial relationships that could be construed as a potential conflict of interest.

Publisher's Note: All claims expressed in this article are solely those of the authors and do not necessarily represent those of their affiliated organizations, or those of the publisher, the editors and the reviewers. Any product that may be evaluated in this article, or claim that may be made by its manufacturer, is not guaranteed or endorsed by the publisher.